Advances in
Geo-Energy Research

Vol. 16, No. 3, p. 260-275, 2025

Original article

Enhancing fracture geometry monitoring in hydraulic fracturing using radial basis functions and distributed acoustic sensing

Shaohua You[1], Qinzhuo Liao[1]*, Yunzhi Yue[1], Shouceng Tian[1], Gensheng Li[1], Shirish Patil[2]

[1]National Key Laboratory of Petroleum Resources and Engineering, China University of Petroleum, Beijing 100249, P. R. China
[2]College of Petroleum Engineering & Geosciences, King Fahd University of Petroleum and Minerals, Dhahran 31261, Saudi Arabia

Keywords:
Fiber optic sensing
distributed acoustic sensing
radial basis function
hydraulic fracturing
fracture inversion

Cited as:
You, S., Liao, Q., Yue, Y., Tian, S., Li, G., Patil, S. Enhancing fracture geometry monitoring in hydraulic fracturing using radial basis functions and distributed acoustic sensing. Advances in Geo-Energy Research, 2025, 16(3): 260-275.
https://doi.org/10.46690/ager.2025.06.06

Abstract:
Accurate identification of fracture geometry in hydraulic fracturing is essential for understanding fracture propagation, optimizing stimulation design, and predicting production performance. Distributed acoustic sensing, as a high-resolution near-wellbore monitoring technique, provides rich spatiotemporal data for real-time observation of fracture responses. However, reconstructing fracture geometry from distributed acoustic sensing measurements remains challenging due to high model dimensionality, ill-posed inversion processes and substantial computational costs. This study presents a fracture geometry inversion framework based on radial basis function, in which the fracture width distribution is represented using a small number of radial basis function modes. Owing to the intrinsic smoothness and symmetry of radial basis function, the method eliminates the need for explicit regularization terms, thereby simplifying the objective function and improving inversion stability. This approach significantly reduces the number of inversion parameters while enhancing both accuracy and physical consistency. Applications to a synthetic benchmark model and real field data from the hydraulic fracturing test site demonstrate that the radial basis function-based method consistently outperforms conventional full-parameter inversion approaches, in terms of fitting accuracy and computational efficiency. The proposed method provides a structurally informed and computationally efficient modeling framework for high-dimensional fracture inversion, offering a promising solution for real-time fracture monitoring and parameter estimation in hydraulic fracturing operations.

1. Introduction

In the development of unconventional hydrocarbon resources, low-permeability formations such as shale and tight reservoirs have emerged as critical energy supplements (Feng et al., 2020). Due to their low porosity and permeability, conventional extraction techniques fail to yield economic production rates, making hydraulic fracturing a key strategy for enhancing reservoir productivity (Liao et al., 2024). By conducting fluid injection under triaxial stress conditions to initiate a complex fracture network and preserve fracture connectivity, this approach enhances fluid drainage and flow efficiency, particularly in shale formations (Abdelaziz et al., 2023). With the growing emphasis on "precision fracturing" and "intelligent monitoring", greater demands have been placed on the accuracy and timeliness of fracture propagation monitoring, control and inversion (Sun et al., 2023).

Accurate identification of fracture geometry plays a crucial role in optimizing stimulation parameters, evaluating reservoir performance, and predicting production outcomes. Real-time monitoring has thus become essential to ensure the effective-

Yandy Scientific Press

*Corresponding author.
E-mail address: 2023310131@student.cup.edu.cn (S. You); liaoqz@cup.edu.cn (Q. Liao); 2023215183@student.cup.edu.cn (Y. Yue); tscsydx@163.com (S. Tian); ligs@cup.edu.cn (G. Li); patil@kfupm.edu.sa (S. Patil).

Received April 2, 2025; revised April 28, 2025; accepted May 15, 2025; available online May 20, 2025.

ness of hydraulic fracturing. A variety of diagnostic methods, including microseismic events, tiltmeter data, tracer flowback and pressure-based interpretations, have been employed to estimate fracture location, size, complexity and proppant distribution in unconventional reservoirs (Mahmoud et al., 2021; Eyinla et al., 2023). However, these methods often suffer from low sensitivity, limited spatial resolution, strong dependence on modeling assumptions and high deployment costs. Microseismic monitoring is subject to image point nonuniqueness and directionally dependent relocation accuracy due to the limited spatial variation in borehole observation geometry (Zhang et al., 2023). In recent years, the advancement of distributed fiber-optic sensing technologies has enabled a new era of high-resolution, full-well, real-time monitoring of fracture behavior. Distributed Acoustic Sensing (DAS) captures strain and vibration signals along the wellbore, enabling analysis of fracture growth paths, propagation velocity, cluster interference and stimulated volume efficiency (Hudson et al., 2021; Staněk et al., 2022). Distributed Temperature Sensing (DTS) tracks thermal distributions and flowback dynamics, which can be used to infer fluid allocation and proppant deposition across clusters (Bertulessi et al., 2022). The combined use of DAS and DTS greatly enhances the completeness and resolution of fracture diagnostics, particularly in complex multi-cluster scenarios (Denney, 2012). Compared to conventional approaches, fiber-optic systems offer high temporal resolution, full-well coverage and independence from downhole power, enabling real-time detection of micro-fracture-induced strain signals (Moradi et al., 2022; Wang et al., 2022a). In horizontal wells, multilayer completions, or staggered fracturing operations, DAS can detect fracture hits in adjacent wells through cross-well coupling and strain array analysis (Wu et al., 2020; Wang et al., 2024; Tegtow et al., 2025). The results from DAS/DTS systems can also be used to calibrate three-dimensional (3D) geomechanical models and fracture simulators, significantly improving the reliability of fracture design and forecasting (Zhang et al., 2020; Wu et al., 2021). Despite challenges in cost, installation complexity and interpretation standardization, fiber-optic monitoring is gaining momentum in unconventional field deployments, becoming a key enabler of real-time inversion and intelligent diagnostics (Chen et al., 2016; Sherman et al., 2019; Al-Jahdhami et al., 2021). In this context, DAS-based interwell monitoring has emerged as a cornerstone for advanced hydraulic fracture diagnostics.

Given the observed time-lapse seismic responses and the need to invert for fracture effectiveness at each stage, constructing physically realistic models becomes critical for interpreting DAS measurements during hydraulic stimulation (Byerley et al., 2018). These models provide the mechanical foundation for hydraulic fracturing and directly influence the accuracy of fracture geometry prediction, proppant placement and production evaluation (Zhang et al., 2017; Tang et al., 2019b; Xi et al., 2021). Classical models such as the Perkins-Kern-Nordgren (PKN) and Khristianovic-Geertsma-de Klerk (KGD) models are widely used to approximate the development of fracture geometry, with the PKN model commonly applied in cases of height-limited fractures and the KGD model representing length-dominated propagation (Xiang, 2012). The pressurized penny-shaped fracture, often referred to as the Fialko model, provides an idealized yet effective representation of radially symmetric near-wellbore fractures under elastic conditions (Paknia et al., 2019). However, it fails to account for the complexity of heterogeneous reservoirs and variable stress conditions. To enhance fracture design adaptability in multilayer formations, the pseudo-3D approach integrates variable fracture height within a two-dimensional (2D) framework by discretizing containment layers and coupling Unified Fracture Design with fracture propagation and linear elastic fracture mechanics models (Yang et al., 2012). Further refinements include the use of linear elastic fracture mechanics theory to estimate maximum fracture height (Garavand and Podgornov, 2018), incorporation of vertical viscous dissipation and two-dimensional flow coupling (Weng, 1992). While the pseudo-3D model offers a balance of complexity and computational efficiency, it still struggles in highly heterogeneous formations. This has led to the rapid development of planar 3D and full 3D models. Tang et al. (2019a) introduced a fully 3D Displacement Discontinuity Method (DDM) that simulates the mechanical interaction and asymmetric propagation of multiple fractures in three-dimensional space, thereby addressing the limitations inherent in traditional 2D models. The phase field method has also been introduced, e.g., Zhuang et al. (2023) proposed a Biot-based 3D phase field model for layered formations that successfully captures fracture deflection, branching and trans-layer penetration. Meanwhile, coupled DDM and finite element methods have emerged to improve accuracy and efficiency through explicit bidirectional coupling (Paullo et al., 2022). Fracture modeling has advanced from analytical approaches with simplifying assumptions, such as constant fracture height in the PKN and KGD models, toward planar 3D and unconventional models that incorporate geomechanical behavior, geological heterogeneity and fluid dynamics. The choice of simulation method continues to reflect a trade-off between physical realism and computational cost, forming the basis for realistic fracture prediction and large-scale reservoir applications (Ismail and Azadbakht, 2024).

In recent years, substantial progress has been recorded, and numerical simulation is a potential tool for developing geometric inversion models based on low-frequency DAS strain data. Liu et al. (2020a) developed the Green's function-based inversion model attempting to solve a linear system for fracture-width inversion near the monitor well, thereby laying the groundwork for later studies. This methodology was subsequently expanded to encompass multi-cluster, multi-stage fracturing scenarios and validated with field data, showcasing its ability to resolve total fracture width and temporal trends in individual fractures (Liu et al., 2021a, 2021b, 2024). Subsequent investigations confirmed that fracture width remains highly sensitive to strain, whereas height inversion is difficult because low-frequency band is directly related to strain only within limited height scenarios (Wu et al., 2021). To enhance inversion accuracy, researchers incorporated Markov chain Monte Carlo based Bayesian frameworks and temporally constrained optimization algorithms for joint inversion of width and height (Liu et al., 2020b; Hu et al., 2023), addressing issues such as low signal-to-noise ratios and cluster interference in field datasets (Moradi et al., 2022). Studies also emphasize that recognizing the heart-shaped pattern from a fracture approaching the fiber is essential for reliable identification of fracture hits (Zhang et al., 2020; Srinivasan et al., 2023). Employing field data from the Hydraulic Fracture Test Site (HFTS) project as a benchmark, several studies have successfully reconstructed multi-well, multi-stage fracture geometries (including width, height and density), facilitating quantitative assessment of inter-well interference and completion design effectiveness (Leggett et al., 2023; Mjehovich et al., 2024). Recently, scholars have begun to train and test deep learning algorithms for far-field strain reconstruction and fracture-geometry prediction (Gurjao et al., 2022). Although forward modeling streamlines the interpretation task, current inversion schemes still suffer from excessive degrees of freedom that cause non-uniqueness and poor computational feasibility. These issues are especially pronounced in cases involving overlapping clusters, asymmetric growth, or distant monitoring wells, where the inversion process becomes highly nonlinear with a high-dimensional parameter space. This often results in slow convergence and error accumulation, making it difficult to meet the demands of real-time data processing in hydraulic fracturing monitoring. Therefore, the development of low-dimensional, robust inversion frameworks that balance physical accuracy with computational efficiency remains a critical challenge.

To address the high dimensionality and computational expense associated with current fracture geometry inversion methods, this study proposes a novel approach based on Radial Basis Function (RBF) dimension reduction. The method encodes the fracture width field using a small number of Gaussian RBFs, which significantly reduces the number of inversion parameters while preserving key geometric features. Unlike traditional methods, the RBF formulation inherently enforces geometric smoothness and symmetry, eliminating the need for explicit penalty functions. This simplification not only enhances inversion stability but also streamlines objective function construction. Benchmark tests show that the RBF-based approach achieves higher fitting accuracy while substantially reducing computation time. These results establish a robust modeling framework for real-time fracture inversion from DAS measurements and provide a promising pathway toward intelligent hydraulic fracturing and real-time closed-loop control in unconventional reservoirs.

2. Method

2.1 Radial basis function

In fracture geometry inversion, traditional approaches typically optimize the fracture width at each grid node independently. While this high-dimensional modeling strategy offers strong representation capability, it suffers from severe drawbacks, including the curse of dimensionality, non-uniqueness and overfitting, which collectively limit its applicability in real-time and stable fracture monitoring. To address these issues, a reduced-order parameterization scheme based on RBF is introduced, which compresses the dimension of the fracture width field using a small number of physically interpretable parameters, thereby enhancing both structural representation and computational efficiency. They have been known, tested and analyzed for several years now, and many positive properties have been identified.

RBFs are spatial interpolation and approximation methods constructed from distance-based kernel functions centered at specific points in the domain. Classical RBF types include Gaussian, thin-plate splines and polynomial functions. Among them, Gaussian RBFs are widely adopted in geophysical modeling, image reconstruction and inverse problems, due to their excellent smoothness, compact support and analytical tractability (Buhmann, 2000). The general form of a Gaussian RBF is given by:

$$w(x) = a \cdot \exp\left(-\frac{\|x-c\|^2}{r^2}\right) \tag{1}$$

where x is the spatial coordinate, c denotes the center of the kernel, r is a scale parameter controlling the spread, and a is an amplitude factor determining the strength of the response. This function is radially symmetric, spatially localized and continuously differentiable, so the interpolation requirements lead to a positive definite interpolation matrix, guaranteeing unique coefficients.

In this study, considering the typical physical characteristics of hydraulic fractures, a Gaussian RBF is adopted to represent the 2D fracture aperture field $w(x,z)$. Since the focus is on modeling the response of a single fracture, a simplified single-kernel Gaussian formulation is employed to minimize the number of parameters and enhance inversion efficiency. The fracture aperture is modeled as:

$$w(x,z) = a_f \cdot \exp\left(-\frac{x^2}{r_x^2} - \frac{z^2}{r_z^2}\right) \tag{2}$$

where a_f denotes the peak aperture, and r_x and r_z are scale parameters that control the extent of the fracture in the horizontal (x) and vertical (z) directions, respectively. The fracture is assumed to be centered at the monitoring well and extends within the $x-z$ plane. The amplitude and shape of the fracture are fully governed by these three parameters.

This RBF model offers several advantages. First, its inherent spatial smoothness and symmetry naturally satisfy geometric regularity without requiring additional penalty terms for continuity or symmetry. Second, it reduces the number of inversion parameters to only three, compared to hundreds in traditional grid-based models, significantly improving optimization stability and convergence. Third, the localized sensitivity of the Gaussian kernel allows it to capture subtle strain variations, especially those recorded by DAS near offset wells, enabling precise reconstruction of fracture-induced heterogeneous strain fields.

To further evaluate the robustness of the proposed RBF-based fracture modeling, a parameter sensitivity analysis was performed. By perturbing the initial values of the amplitude and scale parameters (a, r_x, r_z) within a reasonable range ($\pm$20%), the resulting fracture aperture fields and predicted strain responses were compared. The inversion results exhibited minor variations in fracture geometry and strain distri-

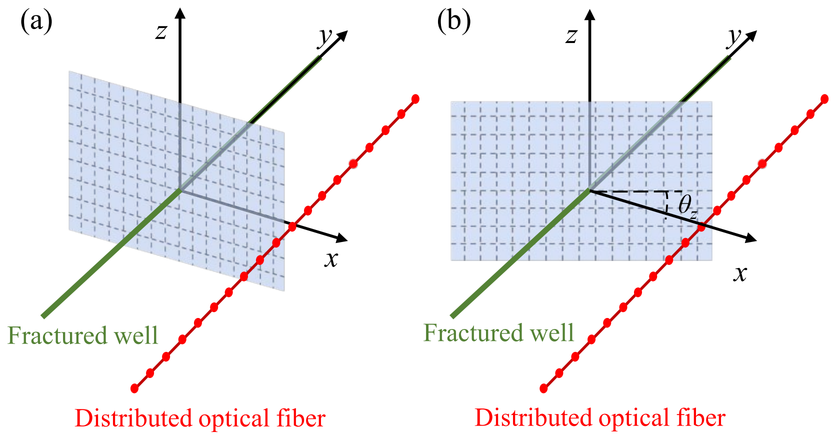

Fig. 1. Schematic of distributed fiber optic monitoring of fractures: (a) Fracture without rotation and (b) fracture plane rotated around the z-axis.

bution, confirming that the model is relatively insensitive to moderate parameter changes. This demonstrates the stability and practical applicability of the Gaussian RBF formulation in realistic inversion scenarios.

In summary, the proposed Gaussian RBF-based fracture modeling approach substantially reduces inversion dimensionality while preserving strong geometric expressiveness and physical realism. Its compact structure, minimal parameterization and computational tractability make it well-suited for DAS-driven fracture inversion, particularly in scenarios requiring real-time monitoring or rapid field diagnostics. This method provides a robust foundation for building efficient and stable inversion frameworks in unconventional reservoir development.

2.2 Fiber-optic strain response

DAS is a high-resolution fiber-optic monitoring technology that measures dynamic strain or strain rate variations continuously along the length of the wellbore. In hydraulic fracturing operations, optical fibers deployed in offset wells can record strain perturbations induced by fracture propagation, providing a physical basis for reconstructing fracture geometry. Compared with traditional indirect techniques such as microseismic monitoring, DAS offers higher spatial sampling density and quantitative measurement capabilities, with notable advantages in detecting fracture hits, inter-cluster interactions, and propagation path deviations near the monitoring well.

In this study, assume a vertical fracture for a horizontal well extends in a two-dimensional $x-z$ plane with $y=0$. The fracture-induced displacement at any fiber-optic monitoring location $u(x_f,y_f,z_f)$ is modeled using a Green function-based kernel formulation, derived from the three-dimensional linear elastic theory as:

$$u(x_f,y_f,z_f)=\oint_{\Omega} G(x_f-x,y_f,z_f-z)\cdot w(x,z)\,\mathrm{d}x\mathrm{d}z \tag{3}$$

where (x_f,y_f,z_f) denote the coordinates of the fiber-optic sensing point, Ω is the fracture plane, w is the fracture width. The Green function G, which is the kernel weight between the fracture point and the fiber point, describes the displacement at a fiber-optic location caused by a unit aperture over the fracture surface as (Shou, 1993):

$$G(x,y,z)=-\frac{2(1-\nu)I_1(x,y,z)-z\cdot I_2(x,y,z)}{2} \tag{4}$$

where ν is the Poisson's ratio of the rock, and

$$I_1(x,y,z)=-\frac{\displaystyle\int_{\Omega}\tan^{-1}\left[\frac{(x_f-x)(z_f-z)}{y_f r}\right]\mathrm{d}x\mathrm{d}z}{4\pi(1-\nu)} \tag{5}$$

$$I_2(x,y,z)=\frac{\displaystyle\int_{\Omega}\tan^{-1}\frac{(x_f-x)(z_f-z)(y_f^2+r^2)}{r\left[y_f^2+(x_f-x)^2\right]\left[y_f^2+(z_f-z)^2\right]}\mathrm{d}x\mathrm{d}z}{4\pi(1-\nu)} \tag{6}$$

where $r=\sqrt{(x_f-x)^2+y_f^2+(z_f-z)^2}$ is the distance from a fracture point (x, z) to a monitoring point $(x_f,\ y_f,\ z_f)$.

Then, the axial strain along the fiber can be computed by the spatial derivative of the displacement field projected onto the fiber direction:

$$\varepsilon(y_f,t)=\frac{\partial u(y_f,t)}{\partial y_f} \tag{7}$$

In practice, since the fiber is discretized into N_f evenly spaced measurement points over a total length L_f, the strain is numerically approximated using a finite difference scheme:

$$\varepsilon_i^t\approx\frac{u_{i+1}^t-u_i^t}{\Delta y},\quad \Delta y=\frac{L_f}{N_f} \tag{8}$$

In practical reservoir settings, the position of a fracture relative to the monitoring fiber is not fixed but often exhibits rotation and translation along the z-axis, both of which significantly influence the measured strain response (Fig. 1). In this study, fracture rotation is modeled by an angular deviation θ_z about the z-axis, representing deflection of the fracture plane within the vertical section. The rotated fracture coordinates are given by:

$$\mathbf{X}_r=\mathbf{R}_z\cdot\mathbf{X}_f \tag{9}$$

where the z-axis rotation matrix $\mathbf{R}_z$ is defined as:

Table 1. Comparison of inversion methods.

No.	Method	Inversion variables	Penalty terms	Equation
1	fit(w)	w	symmetry, smoothness, temporal continuity	(14)
2	fit($w+\theta_z$)	w, θ_z	symmetry, smoothness, temporal continuity	(15)
3	fit($\mathrm{RBF}+\theta_z$)	a, r_x, r_z, θ_z	temporal continuity	(16)

$$\mathbf{R}_z = \begin{bmatrix} \cos\theta_z & -\sin\theta_z & 0 \\ \sin\theta_z & \cos\theta_z & 0 \\ 0 & 0 & 1 \end{bmatrix} \tag{10}$$

where $\mathbf{X}_f$ denotes the original coordinates of the fracture in the global reference frame, and $\mathbf{X}_r$ represents the transformed coordinates after applying the rotation.

In summary, the fiber-recorded strain primarily captures the dynamic displacement field induced by fracture propagation in the vicinity of the wellbore. Its magnitude and spatial distribution are jointly controlled by fracture width, length, and spatial positioning. Consequently, the strain waterfall observed in DAS measurements serves as an indirect signature of fracture geometry evolution, offering a physically grounded basis for geometry inversion.

2.3 Inversion method

In conventional fracture geometry inversion, the standard approach directly optimizes the fracture aperture at each grid node. Although this high-dimensional formulation offers considerable representational flexibility, it also introduces severe challenges including ill-posedness, local minima entrapment, and excessive computational cost. To constrain the solution space and ensure physical plausibility, symmetry and smoothness penalty terms are often added to the loss function (Liu et al., 2021a):

$$\begin{aligned} L_{\mathrm{g}} &= \lambda_y \cdot \oint_\Omega [w(x,z) - w(-x,z)]^2 \,\mathrm{d}x\mathrm{d}z + \\ &\lambda_m \cdot \oint_\Omega \left[\left(\frac{\partial w}{\partial x}\right)^2 + \left(\frac{\partial w}{\partial z}\right)^2 \right] \mathrm{d}x\mathrm{d}z \end{aligned} \tag{11}$$

where λ_y and λ_m are weighting coefficients that control the influence of the symmetry and smoothness constraints in the total geometric loss. The corresponding objective function J_d can be written as:

$$J_d = \oint_\Omega [\varepsilon_m - \varepsilon_p(w(x,z))]^2 \,\mathrm{d}x\mathrm{d}z + L_g \tag{12}$$

where ε_m denotes the measured strain, and $\varepsilon_p(w)$ represents the predicted strain based on a given fracture width distribution w. The predicted strain $\varepsilon_p(w)$ is computed based on Eqs. (3)-(8). To improve temporal consistency in the inversion process, a penalty is introduced that minimizes the difference in aperture fields between adjacent time steps:

$$L_t = \lambda_t \cdot \int_0^T \mathrm{d}t \oint_\Omega \left[\frac{\partial w(x,z,t)}{\partial t}\right]^2 \mathrm{d}x\mathrm{d}z \tag{13}$$

where T is the end of time, and λ_t is the weight controlling the strength of temporal regularization. The complete objective function J_w is then written as:

$$J_w = J_d + L_t \tag{14}$$

The inversion framework is further enhanced by incorporating a geometric parameter θ_z, which represents the rotation angle of the fracture around the z-axis. This parameter is used to account for the relative orientation between the fracture and the monitoring fiber, thereby enhancing the inversion's ability to capture spatial variations in geometric configuration, particularly in scenarios involving structural complexity and asymmetric fracture propagation. At this stage, the corresponding loss function is expressed as follows:

$$J_{w+\theta_z} = \oint_\Omega [\varepsilon_m - \varepsilon_p(w(x,z,\theta_z))]^2 \,\mathrm{d}x\mathrm{d}z + L_g + L_t \tag{15}$$

A dimension-reduction strategy based on RBF is proposed in this study, aiming to simplify the objective function while enhancing inversion stability and efficiency. The RBF formulation uses a small set of interpretable parameters to approximate the continuous aperture field, inherently enforcing smoothness and symmetry without requiring explicit penalty terms. Thus, combining Eqs. (2) and (15), the proposed RBF-based loss function is expressed as:

$$J_{\mathrm{RBF}+\theta_z} = \oint_\Omega \left[\varepsilon_\mathrm{m} - \varepsilon_\mathrm{p}(a, r_x, r_z, \theta_z)\right]^2 \mathrm{d}x\mathrm{d}z + L_t \tag{16}$$

In order to systematically compare the performance of different inversion strategies, three distinct schemes are tested (Table 1):

1) Method 1 uses the whole fracture width field as the inversion variable and includes penalties on symmetry, smoothness and temporal continuity, as in Eq. (14).
2) Method 2 incorporates both fracture width and θ_z as inversion variables, while retaining the same three penalty terms, as in Eq. (15).
3) Method 3 employs the RBF parameters (amplitude, horizontal and vertical spread) and θ_z as the inversion variables, using only a single penalty term to enforce temporal consistency, as in Eq. (16).

The optimization problem is solved using the fminunc function in MATLAB, which implements the quasi-Newton algorithm suitable for unconstrained nonlinear optimization problems with continuously differentiable objective functions. Compared to global optimization techniques, the quasi-Newton algorithm is more efficient for problems of moderate dimensionality, especially when good initial guesses are avail-

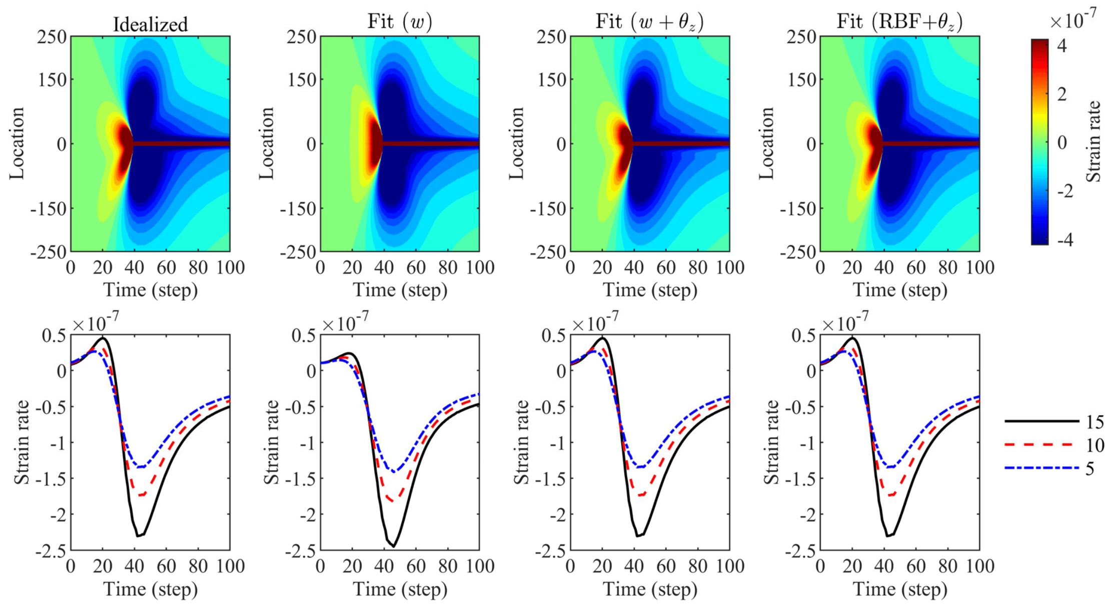

Fig. 2. Comparison of strain rate distributions and typical point responses under the synthetic model using different inversion methods.

able, such as using the solution from the previous time steps. In this study, the initial guess for each time steps is set as the optimized solution from the previous step, while the initial guess for the first step is manually specified based on physical estimates. The convergence criteria are defined by a maximum of 30,000 iterations, a function tolerance of 1×10^{-10}, and an optimality tolerance of 1×10^{-16}. By properly configuring parameters such as the number of iterations, tolerance limits and gradient accuracy, the quasi-Newton algorithm is able to reliably converge to a local optimum and achieve high-fidelity fitting of the spatial distribution of strain. For more complex inversion problems involving highly nonconvex objectives or multiple RBF kernels, global optimization algorithms such as differential evolution, genetic algorithms, or particle swarm optimization could be explored to improve robustness against local optima, albeit at the cost of higher computational demand.

In summary, this work establishes an RBF-based fracture inversion framework that simplifies the objective function while significantly reducing the dimensionality of the parameter space and computational burden. Compared with conventional methods, the inherent smoothness and symmetry of the RBF representation eliminate the need for additional geometric constraints, thereby improving the stability and physical consistency of the inversion. This approach provides a practical and efficient solution for real-time fracture geometry monitoring using distributed fiber sensing in hydraulic fracturing operations.

3. Applications and results

To comprehensively assess the performance advantages of the proposed RBF-based fracture inversion strategy in terms of accuracy and efficiency, this section presents a three-pronged evaluation. First, controlled inversion experiments are conducted on a synthetic fracture model to compare the geometric reconstruction and parameter recovery capabilities of the proposed method with those of traditional direct width fitting approaches. Second, two representative field datasets from the HFTS hydraulic fracturing site are used to test the robustness and adaptability of the method under realistic conditions with measurement noise. Finally, for all inversion schemes, the computational time and resource usage are systematically benchmarked to evaluate their feasibility for real-time fracture monitoring. These experiments, encompassing both synthetic and field conditions, aim to validate the proposed method's comprehensive performance in terms of inversion accuracy, stability and computational cost.

3.1 Synthetic model

An analytically defined fracture field based on the classical Perkins-Kern-Nordgren model was constructed to serve as the ground-truth reference for inversion performance evaluation. This model assumes symmetric fracture propagation in the horizontal direction, with the width distribution governed by elastic and injection parameters, and a constant vertical height. The resulting fracture exhibits a smooth, continuous, and symmetric geometry, making it a well-suited benchmark for method comparison under controlled, interpretable conditions.

The inversion results for the strain rate field under the synthetic model are presented in Fig. 2. The reference scenario simulates a fracture rotated 15° about the z-axis, yielding a spatially asymmetric strain rate field concentrated on one side of the monitoring well. The upper row shows the spatiotemporal distribution of strain rate along the well trajectory, while the lower row provides strain rate time series at three representative offsets (d = 5, 10 and 15 m). Results from the first method (second column) exhibit an overly symmetric strain distribution, failing to capture the spatial asymmetry

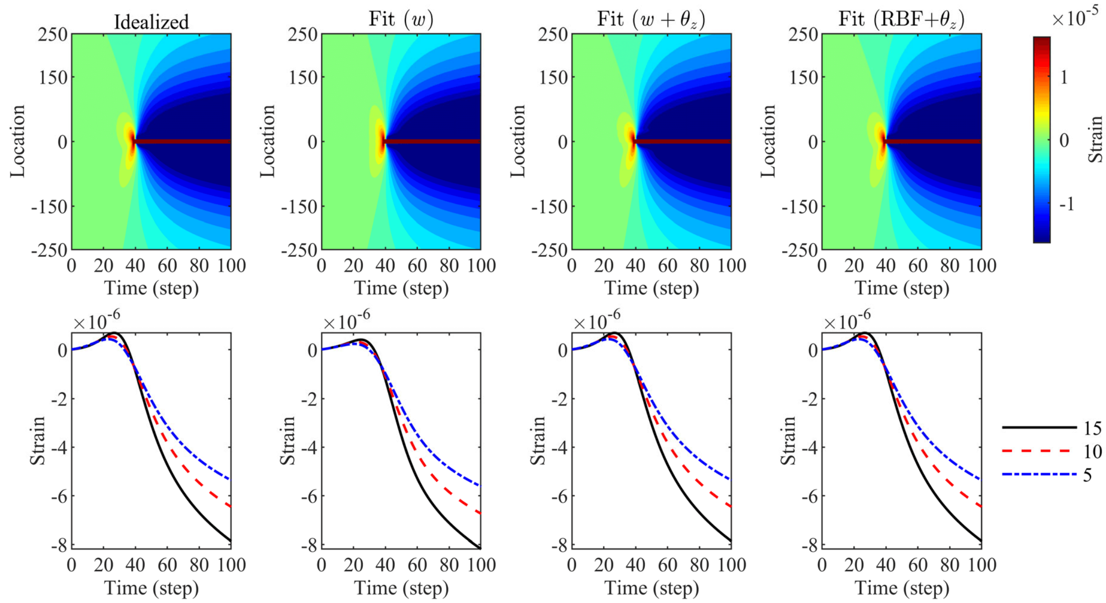

Fig. 3. Comparison of strain distributions and typical point responses under the synthetic model using different inversion methods.

induced by the fracture rotation. Although the overall amplitude and trend of the time series align reasonably well with the reference, substantial spatial deviations are observed. The second method (third column), with the added geometric rotation parameter, more accurately reconstructs the asymmetric pattern and achieves better alignment with the ground truth in terms of perturbation location and intensity. The proposed RBF method (fourth column) demonstrates the most accurate recovery, reproducing both the spatial asymmetry and temporal dynamics of the strain rate field. The resulting patterns closely match the reference model, with minimal noise and excellent agreement in both amplitude and temporal variation.

The strain distribution results inverted by different methods under the synthetic model are illustrated in Fig. 3. The top row shows the strain waterfall plots along the entire wellbore over time, while the bottom row displays the temporal strain curves at three representative measurement points (d = 5, 10 and 15 m). In this scenario, the fracture is rotated 15° about the z-axis, resulting in a strain response that exhibits clear spatial asymmetry. As shown, the traditional method in the second column adopts the inversion strategy without geometric parameters, which can roughly recover the main fracture-induced strain trend, produce inversion results with non-physical symmetry, inconsistent with the actual rotated fracture geometry, due to the absence of the θ_z parameter. Notably, significant errors are observed near the fracture tip. In contrast, the latter two methods incorporate the geometric parameter θ_z, which greatly improves the spatial resolution of the strain field. The third column, which adds a geometric rotation term to the traditional fracture width inversion, significantly mitigates the symmetry artifacts and aligns more closely with the true pattern. The fourth column shows results from the RBF-based inversion method, which not only reproduces the rotated structure with high fidelity in spatial distribution but also achieves near-perfect agreement with the true strain time series in terms of amplitude and dynamics, demonstrating the superiority of the RBF model in both expressiveness and fitting accuracy.

The inverted strain fields at four key time steps (20, 35, 40 and 50), covering different stages of fracture propagation are shown in Fig. 4. Black solid lines indicate the reference strain values, while the symbols represent inversion results from the three methods: Blue circles for the traditional width fitting, green triangles for fit($w+\theta_z$), and red squares for the RBF-based method. The top-right corner of each plot indicates the relative error ε for each method at the current time steps. In the first three steps, the traditional method shows large deviations due to the lack of θ_z, failing to capture asymmetry caused by fracture rotation, resulting in amplitude imbalances and spatial misalignment. After introducing θ_z, the spatial relation between the fracture and fiber is better resolved, significantly enhancing symmetry and accuracy. The RBF method achieves further improvement, obtaining high-accuracy results through a simple function form and temporal regularization alone, without relying on symmetry or smoothness penalties. It consistently delivers the lowest relative error across all time steps.

The geometric recovery capabilities of the three inversion strategies under the rotated fracture setting are depicted in Fig. 5. The top row depicts 3D spatial relationships between the inverted fractures and the fiber, highlighting whether the fracture rotation (θ_z) is correctly identified. The bottom row presents the 2D fracture profiles at four representative time steps. As observed, the traditional method, lacking θ_z, consistently yields orthogonal fracture orientations, failing to capture the actual rotation and maintaining artificially symmetric shapes. In contrast, methods incorporating θ_z reveal time-evolving rotated profiles consistent with the observed data, recovering physically plausible fracture geometries. Notably,

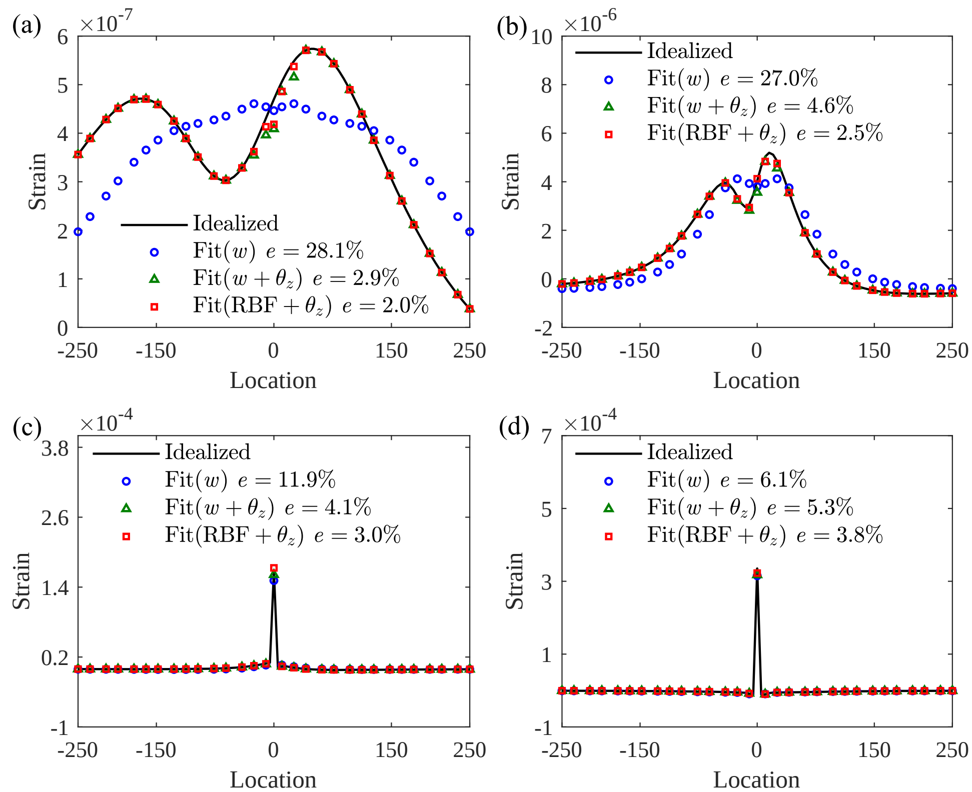

Fig. 4. Comparison of strain distribution at multiple time steps: (a) 20, (b) 35, (c) 40 and (d) 50 under the synthetic model.

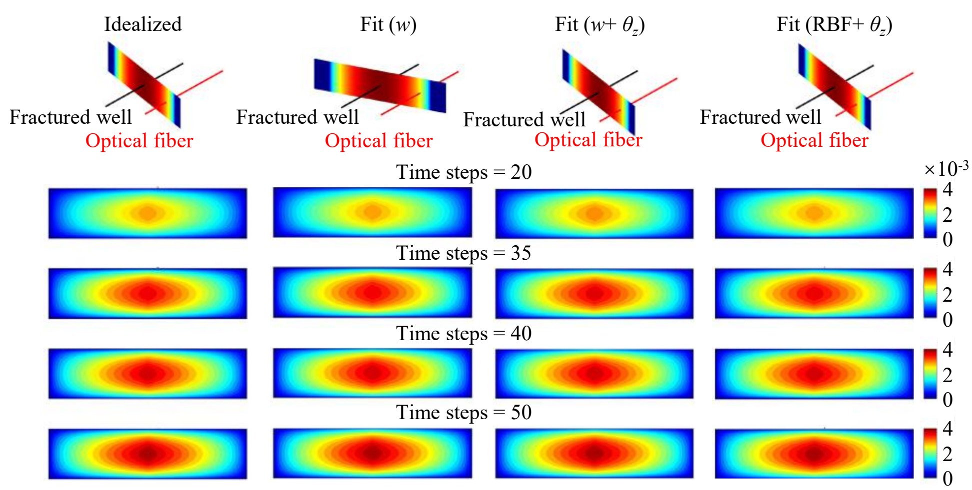

Fig. 5. Comparison of 2D fracture width distributions under the synthetic model using different methods.

the RBF method, despite using no explicit symmetry or smoothness constraints, produces high-quality fracture profiles characterized by smoothness, continuity and structural realism, purely through a compact function form and a single temporal consistency term.

To further quantify inversion accuracy, the fracture width profiles at time steps 20, 35, 40 and 50 across all three methods against the synthetic model are compared in Fig. 6. The black curves represent the reference width distributions, and the symbols denote the corresponding inversion results, with each legend including the relative error for that method. All methods perform well in reconstructing the primary fracture zone, particularly at the fracture center where fitting accuracy is highest. This confirms that the proposed inversion framework is well-suited for detailed fracture geometry modeling. Among them, the RBF method consistently achieves the best results, with reconstructed curves nearly overlapping the reference and maintaining the lowest error across all time steps. This is attributed to the RBF's inherent smoothness and physical consistency, which allows for accurate shape representation even without auxiliary regularization.

In summary, under the synthetic model test, the proposed RBF-based dimension reduction approach exhibits superior performance in terms of inversion accuracy, physi-

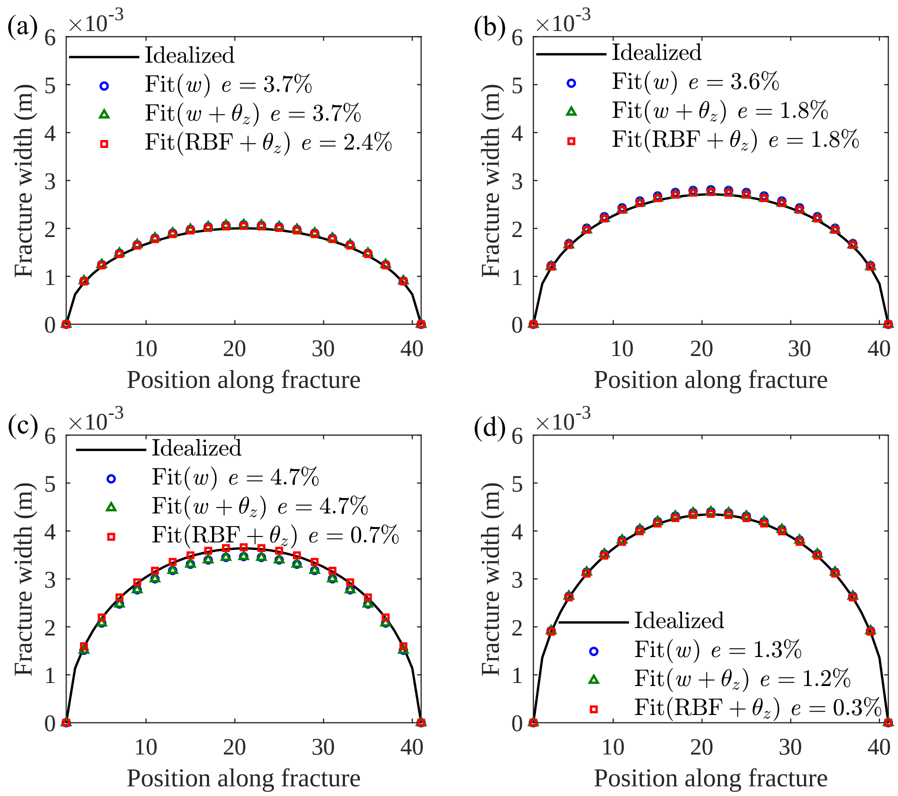

Fig. 6. Comparison of fracture width profiles along the fracture centerline at different time steps: (a) 20, (b) 35, (c) 40 and (d) 50.

cal consistency and parameter compactness. Compared with the traditional direct width fitting method, the RBF strategy reconstructs smooth and symmetric fracture geometries without relying on explicit regularization terms, significantly reducing the complexity of the objective function and easing the optimization process. The introduction of the geometric parameter θ_z further enhances the model's spatial adaptability by correcting relative positional errors between fracture and fiber, leading to improved fitting performance for both strain and strain rate. Overall, the RBF method yields inversion results that align closely with the ground truth in all tested aspects (e.g., strain response, fracture shape and width profile), achieving minimal error and robust structural fidelity. These findings establish a solid foundation for extending the method to real-world DAS datasets.

3.2 Real field data

Following the validation under synthetic conditions, the proposed inversion framework was further applied to real field monitoring data to evaluate its adaptability and robustness under practical and complex operational scenarios. Two datasets (Cases 1 and 2) were selected from the well-known HFTS program (Ciezobka, 2021). These datasets were acquired during in-situ fracturing operations using distributed fiber-optic sensors deployed along monitoring wells. The data are characterized by a high signal-to-noise ratio, fine temporal resolution and short standoff distances between the monitoring fiber and the fracture zone.

The strain-rate distribution and time series responses at representative locations for Case 1 are presented in Fig. 7. The top row shows the full-length strain-rate distribution along the wellbore over time. To examine the role of the rotation angle θ_z in the inversion process, three representative locations were selected at -50, 0 and 50 m to display the strain-rate time histories in the bottom row. The measured waterfall plot reveals a pronounced spatial asymmetry. When comparing the results of the three inversion strategies, the traditional fracture-width fitting method to fit(w) yields a symmetric strain-rate field, with nearly identical responses at -50 and 50 m, failing to capture the asymmetry induced by fracture rotation. In contrast, the inclusion of the geometric parameter θ_z enables both the direct width fitting method and the RBF-based approach to recover the asymmetric features observed in the field data. Notably, in the trailing edge of the fracture where negative strain rates dominate, the RBF method for fit($\mathrm{RBF} + \theta_z$) exhibits superior agreement with the measured amplitude and pattern, and its spatial response closely matches the observed structure. These results demonstrate that the RBF-based method offers stronger morphological adaptability, avoids bias introduced by artificial symmetry and smoothness constraints, and exhibits higher resolution and fidelity when modeling complex field strain signals.

Based on the strain-rate inversion results, the accuracy of the three methods in fitting the strain field itself was further evaluated, as shown in Fig. 8. The figure displays the measured strain distribution and the corresponding results from each

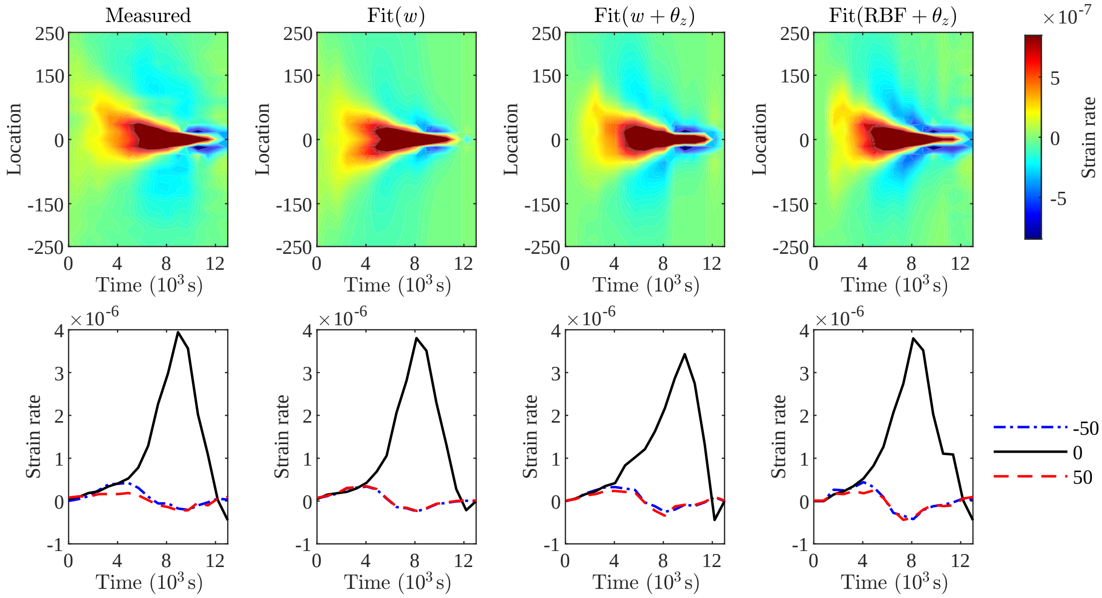

Fig. 7. Comparison of strain rate distributions and typical point responses under the HFTS data (Case 1) using different inversion methods.

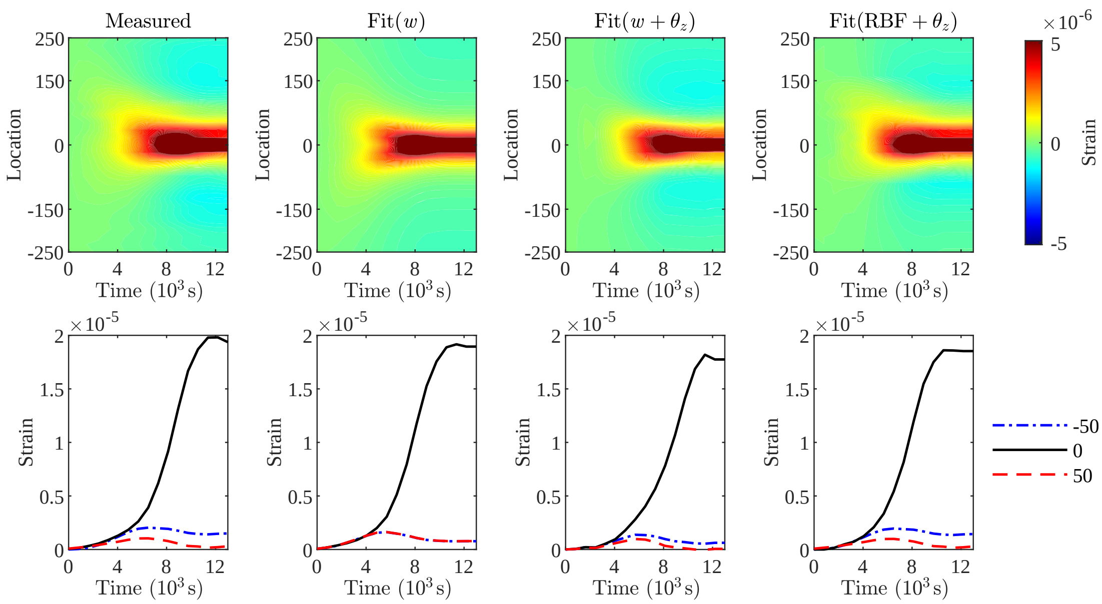

Fig. 8. Comparison of strain distributions and typical point responses under the HFTS data (Case 1) using different inversion methods.

method, along with time-series strain responses at the three key positions (-50, 0, 50 m). Overall, all methods successfully capture the dominant temporal trend in strain accumulation, particularly at the central position (0 m), where the inversion matches the measured trend with high fidelity. However, significant differences emerge in terms of spatial symmetry. The traditional fit(w) method produces nearly identical results at -50 and 50 m, indicating an overly idealized shape assumption that fails to capture the real fracture deflection. In contrast, both fit($w+\theta_z$) method and fit(RBF $+\theta_z$) method, which incorporate the rotation parameter θ_z, generate curves at the edge positions that more closely match the field observations. The RBF-based method is particularly effective in reproducing both the magnitude and detailed features of the measured curves. This comparison confirms that fracture rotation has a strong influence on the strain field in real formations, and accurately recovering such asymmetry requires the introduction of the geometric parameter θ_z. Furthermore, the RBF approach is capable of accurately reconstructing the fracture-induced strain field without the need for symmetry or smoothness penalties, highlighting its robustness and accuracy under complex field conditions.

To further evaluate the strain fitting capabilities of each method at individual time steps, Fig. 9 presents the along-

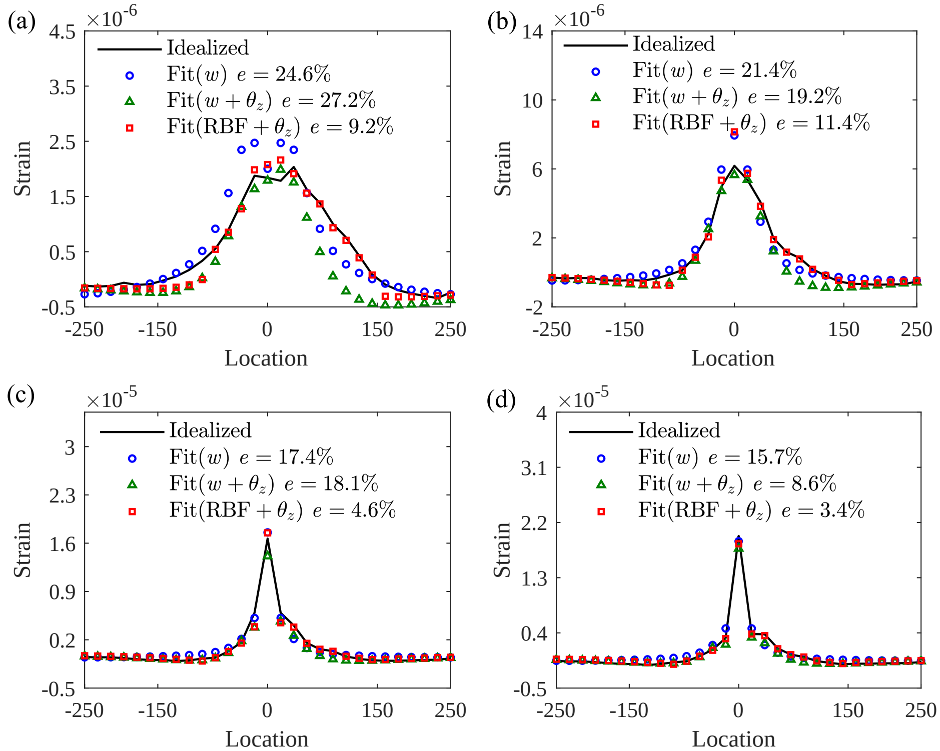

Fig. 9. Comparison of strain distribution at multiple time steps (a) 4,900, (b) 7,300, (c) 9,800 and (d) 12,200 for the HFTS data (Case 1).

well strain distributions and corresponding fitting errors at four representative time points: 4,900, 7,300, 9,800 and 12,200 s. The traditional method exhibits significant errors across all time points, particularly during phases with asymmetric strain distributions or rapid peak variations, where the fitting performance deteriorates. Incorporating θ_z, the fit($w + \theta_z$) method shows overall alignment improvements; however, certain regions still display amplitude deviations and shape discrepancies. In contrast, the RBF method consistently reconstructs the measured strain profiles with higher fidelity across all four time steps. Notably, at 4,900 and 9,800 s (i.e., instances of pronounced perturbations), the RBF method's fitted curves closely match the measured data, with smoother transitions at the boundaries, more accurate peak positions and the lowest errors (9.2% and 4.6%, respectively). A similar trend is observed in Case 2, consistent with Case 1 (see Appendix A in Supplementary file for details).

This section conducted inversion comparison experiments using HFTS field data to evaluate the proposed RBF modeling method's strain and strain rate fitting capabilities under actual monitoring conditions. The results indicate that introducing θ_z as a geometric fitting parameter enables the model to accurately capture the asymmetric strain responses observed in the field data, outperforming traditional methods lacking this parameter. Furthermore, the RBF method reconstructs reasonable strain distributions without relying on symmetry and smoothness penalty terms, demonstrating its inherent constraint capabilities and fitting accuracy. In scenarios with higher data noise or complex strain distributions, the RBF method exhibits greater fitting consistency and robustness. Overall, incorporating θ_z enhances geometric adaptability, while the structural advantages of the RBF method provide solid support for simplifying model construction and improving inversion efficiency.

3.3 CPU time and accuracy

This section further compares the three inversion methods in terms of computational efficiency and fitting accuracy, with a focus on their scalability and engineering applicability for varying fracture mesh resolutions. While the previous section primarily addressed geometric reconstruction and strain matching performance, the current analysis emphasizes the trade-off between speed and accuracy, especially when mesh density increases significantly. The objective is to assess whether each algorithm maintains both accuracy and computational efficiency as resolution demands escalate.

All tests of computational cost and inversion accuracy were conducted using the first set of field-measured strain data from the HFTS project. The computations were performed under identical hardware conditions on a workstation equipped with an AMD Ryzen 7 5800X processor at 3.80 GHz, 16.0 GB RAM, running a 64-bit Windows operating system with x64 architecture. The averaged convergence curves across all time steps for different inversion methods are compared in Fig. 10(a). Overall, all three approaches demonstrate good convergence behavior, successfully minimizing the objective function during iterations. Compared to the traditional width-fitting methods, the proposed RBF-based method achieves lower final objective values, indicating improved optimization

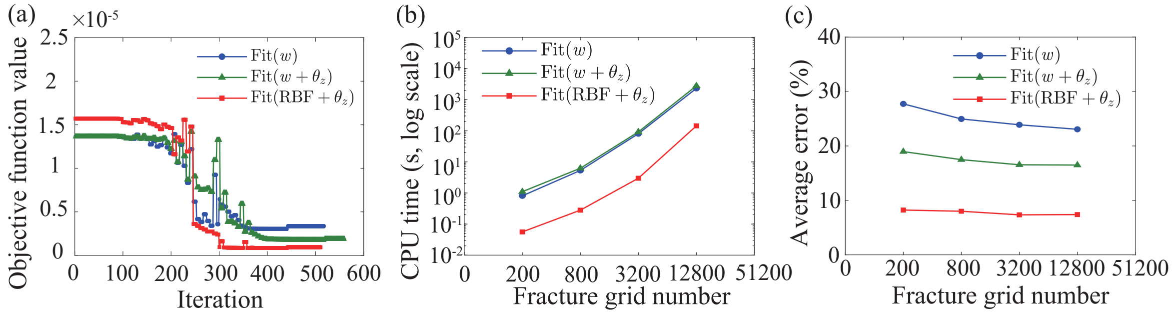

Fig. 10. Comparison of (a) convergence curves of different methods, (b) CPU time and (c) average error with varying fracture grid resolution.

robustness and fitting precision.

The average CPU time per time step (in seconds, log scale) for each inversion method in different fracture mesh resolutions (200, 800, 3,200 and 12,800 gridblocks) and the corresponding average fitting error in the strain field (in percentage) are shown in Figs. 10(b) and 10(c), respectively. It is evident that the traditional direct width-fitting method and its extension with geometric parameters yield nearly identical computational times, both increasing exponentially with mesh resolution. At the highest resolution (12,800 meshes), the per-time-step runtime exceeds 300 seconds, revealing a significant computational bottleneck. In contrast, the proposed RBF-based method maintains consistently low computational time across all mesh conditions, remaining less than 30 seconds even at the highest resolution, thus demonstrating excellent numerical efficiency and scalability.

In terms of accuracy, the RBF method consistently yields the lowest fitting errors across all resolutions, with average error values maintained between 7% and 9%, and showing strong stability. The traditional methods, by comparison, exhibit errors exceeding 20%, and even at high resolutions fail to reduce below a 15% error threshold. These results further confirm that the RBF method, without relying on symmetry or smoothness penalty terms, enhances convergence efficiency while preserving strong representational power and geometric fidelity.

In addition to CPU time, compared to the traditional direct fracture width fitting method, the dimension-reduced fitting approach based on RBF significantly reduces memory usage. Because the RBF model optimizes only a few parameters that are independent of the fracture mesh resolution, memory consumption remains nearly constant even as the mesh becomes denser, whereas the traditional methods experience substantial growth in memory demand. Regarding parallelizability, the RBF inversion framework supports efficient parallel computation across different time steps, as each snapshot inversion is independent. Although the optimization within a single time step is sequential, the lightweight structure of the RBF model allows scalable processing for real-time monitoring and large-scale field applications. Regarding parallelizability, the RBF inversion framework supports efficient parallel computation across different time steps, since each snapshot is optimized independently without temporal dependencies. This enables straightforward deployment on multi-core CPUs or high-performance computing platforms, facilitating acceleration in large-scale or real-time monitoring applications. Although each time step is solved sequentially by default, the compact parameter space and low per-step memory requirements make the method highly scalable and practical for field-scale implementation.

In summary, the inversion strategy proposed in this study offers two key advantages for strain reconstruction tasks: Excellent numerical scalability, enabling fast computation even for high-resolution modeling scenarios; and superior accuracy and robustness, maintaining leading performance across multi-scale tests. These features make the method particularly well-suited for real-time field monitoring and high-frequency data processing applications.

4. Discussion

4.1 Number of RBF basis functions

In this inversion framework, the fracture geometry is modeled using a single Gaussian RBF, based on the observation that most practical hydraulic fractures are single-cluster, approximately symmetric, and smoothly varying. This compact representation effectively captures dominant aperture variations and accurately interpolates strain responses at sensor locations. The method is favored for its localization, smoothness, parameter linearity, and robustness in inverse modeling. However, in more complex cases involving multiple apertures, strong asymmetry, or localized perturbations, a single RBF may be insufficient. In such cases, a superposition of Gaussian kernels with different centers and widths is required to represent the geometry. These multi-kernel models, as nonlinear state-dependent systems, can capture intricate features such as branching and intermittency. In these cases, the aperture $w(x,z)$ can be expressed as a sum of multiple Gaussian RBFs, formulated as:

$$
\begin{aligned}
&w(x,z) = \\
&a_1 \exp\left(-\frac{x^2}{r_{x1}^2} - \frac{z^2}{r_{z1}^2}\right) + a_2 \exp\left[-\frac{(x-x_2)^2}{r_{x2}^2} - \frac{(z-z_2)^2}{r_{z2}^2}\right] + \\
&\cdots + a_n \exp\left[-\frac{(x-x_n)^2}{r_{xn}^2} - \frac{(z-z_n)^2}{r_{zn}^2}\right]
\end{aligned} \tag{17}
$$

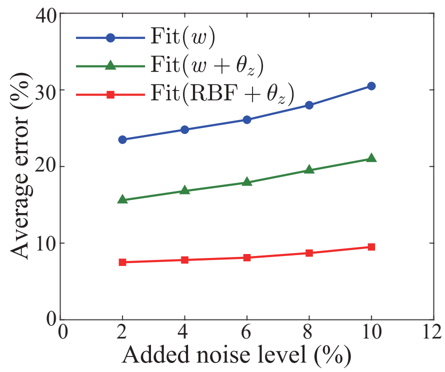

Fig. 11. Comparison of noise sensitivity for different inversion methods.

where a_1, a_2, $\cdots$, a_n are the amplitude parameters, r_{xi}, r_{zi} are the scaling parameters in the x and z directions for the i-th kernel, and (x_i, z_i) denote the center coordinates of the i-th kernel. This general formulation offers flexibility by employing Gaussian kernels, one for each localized feature, thereby depicting complex aperture fields. Although in theory, adding multiple RBFs could enhance the model's representational capacity for more complex geometries (e.g., such as multi-modal apertures, asymmetric propagation and localized boundary perturbations), the results from both synthetic models and real field data in this study suggest that a single RBF already provides accurate reconstruction of primary fracture aperture and positional deviations. Moreover, the condition number of the overlap matrix increases sharply with additional kernels, and fitting error declines little, whereas optimization instability rises markedly.

Introducing multiple basis functions inevitably increases the degrees of freedom and nonlinearity of the inversion problem, making the optimization more prone to local minima and substantially increasing the computational load and convergence time. It can be seen from Fig. 10 that using a single RBF achieves a reasonable balance between accuracy and efficiency. In contrast, more heterogeneous settings, like natural fractures or abrupt facies changes, may benefit from multiple RBFs to capture localized variations. This could extend the method's applicability to complex cases such as intersecting or branching fractures. Future research may explore adaptive strategies, adding extra kernels only where needed, while keeping the global model simple and stable.

4.2 Noise sensitivity analysis

To further evaluate the robustness of the proposed inversion framework under realistic measurement conditions, a noise sensitivity test was conducted. Different levels of synthetic Gaussian noise (2% to 10%) were added to the strain-rate data, and the average inversion errors were assessed for the three methods, as shown in Fig. 11.

All methods exhibit increasing fitting errors with rising noise levels, which is expected. Nevertheless, the RBF-based approach demonstrates the highest robustness, consistently maintaining average errors below 10% even at the highest noise level. In contrast, the traditional width-fitting method (fit(w)) and its extension with geometric parameters (fit($w+\theta_z$)) show larger error increases. Specifically, at 10% added noise, fit($w+\theta_z$) exhibits an average error exceeding 30%, while fit($w+\theta_z$) maintains around 21%. hese results confirm that the dimension-reduced, localized structure of the RBF model offers inherent resilience against measurement noise, avoiding the amplification of noise-induced artifacts across the fracture domain. Therefore, the proposed method not only achieves higher inversion accuracy under ideal conditions but also ensures superior stability and reliability when applied to noisy field data. Additionally, although this study mainly focuses on measurement noise, the inversion framework is expected to maintain reasonable performance under missing data conditions or localized signal degradation, due to the low-dimensional and localized nature of the RBF parameterization. Furthermore, the results under added noise implicitly demonstrate robustness against reduced signal-to-noise ratios, which is common in practical DAS measurements.

4.3 Multi-time-step inversion

The inversion strategy employed in this work is based on independent inversion at each individual time steps, with the fracture geometry being reconstructed separately for each temporal snapshot. To introduce a degree of physical temporal continuity, a penalty term is incorporated in the objective function that constrains the difference in fracture aperture between adjacent time steps, thereby suppressing unrealistic geometric discontinuities. While this approach introduces temporal smoothness at low computational cost, it still has notable limitations: On the one hand, the penalty term relies on hyperparameter tuning, which, if poorly calibrated, can result in either over-smoothing or insufficient constraint; on the other hand, the optimization remains fundamentally sequential, lacking a global modeling framework to capture systematic temporal evolution of the fracture geometry during hydraulic stimulation.

In contrast, a unified multi-time-step inversion strategy, where fracture states across the entire time sequence are estimated simultaneously in a single optimization framework, would enable more comprehensive reconstruction of the fracture evolution process. However, direct high-dimensional representations such as node-wise inversion significantly increase the number of unknowns, leading to higher computational cost, reduced convergence stability, and limited practical use. The use of RBF modeling effectively addresses this challenge. Since each time step can be described with only a few RBF parameters, the overall parameter space is greatly reduced, making joint inversion feasible. In addition, the temporal changes in fracture geometry can be interpreted as trajectories of RBF parameters. This allows the application of temporal regularization, smoothing, or regression-based models to improve stability and physical consistency. The parameter trajectory concept also supports the integration of additional features, including fracture growth rates and stage synchronization.

In summary, the dimension reduction enabled by RBF not only improves the computational efficiency and structural expressiveness of single-step inversion, but also lays a methodological foundation for developing multi-time-step joint inversion strategies. This advancement paves the way for transitioning from static geometry identification to dynamic process modeling, thus supporting the evolution of hydraulic fracture monitoring toward real-time and intelligent analysis.

4.4 Dimension reduction methods

Dimension reduction is a key strategy for addressing the challenges of high-dimensional fracture inversion, aimed at capturing the maximum variance with the fewest parameters. Common dimension reduction techniques include Principal Component Analysis (PCA), Singular Value Decomposition (SVD) and Discrete Cosine Transform (DCT). Each of these methods has its own strengths across various applications, but they also present clear limitations in the context of fracture geometry inversion.

PCA and SVD are classical data-driven techniques that extract orthogonal directions of maximum variance from large datasets. While effective in image and speech recognition, their performance depends on abundant, high-quality training samples. In near-well DAS fracture inversion, however, the fracture geometry is unknown, making such training infeasible. As a result, PCA and SVD are ill-suited for unsupervised scenarios, often producing mode mismatches and structural distortions that reduce reconstruction accuracy and interpretability. In contrast, DCT is a training-free analytical method using fixed orthogonal cosine bases ordered by frequency. It effectively compacts energy and preserves boundary continuity in natural signals. However, due to its symmetric and global basis structure, DCT performs poorly in representing asymmetric or offset geometries. This often leads to artificial symmetry and block artifacts, manifesting as non-physical “M-shaped” fracture profiles with central depressions and raised edges. These artifacts degrade inversion fidelity and are difficult to eliminate, even with a large number of modes.

In contrast, the RBF approach used in this study offers a mesh-free interpolation scheme and demonstrates significant advantages in both expressiveness and adaptability. It models geometries using localized Gaussian kernels, achieving accurate fracture reconstruction with a single RBF, thus avoiding mode mixing and redundant parameters. Unlike PCA or SVD, it does not require statistical training, and unlike DCT, it is more suitable for irregular or asymmetric fractures due to its reliance solely on Euclidean distance. In summary, RBF removes dependence on training data or fixed modes, offering greater flexibility and physical consistency, which makes it ideal for real-time inversion with sparse data and unknown geometries. It provides a robust, efficient, and scalable solution for hydraulic fracture monitoring in complex subsurface conditions.

5. Conclusions

Accurate reconstruction of fracture geometry in hydraulic fracturing is critical for understanding stimulation mechanisms, optimizing operational parameters and evaluating treatment effectiveness. DAS, as a high-resolution and long-reach downhole monitoring technology, has been widely adopted for near-wellbore fracture diagnostics. However, translating DAS strain data into reliable fracture geometries remains a major challenge due to high parameter dimensionality, model freedom and inversion instability. To address these issues, this paper proposes a dimension-reduced inversion framework based on RBF. By using RBF to represent fracture profiles, the method significantly compresses the parameter space while preserving structural integrity. Its performance is validated through both synthetic models and real field data from the hydraulic fracturing test site project, and systematically compared against traditional full-dimensional inversion techniques.

Experimental results demonstrate that the proposed method achieves high accuracy and stability across both synthetic and field datasets. While maintaining competitive fitting precision, the RBF approach substantially reduces parameter complexity and computational time, particularly in high-resolution scenarios. Unlike traditional methods, RBF requires no explicit symmetry or smoothness penalty terms, as its kernel formulation naturally yields physically realistic, smooth fracture shapes. Moreover, in contrast to statistical dimension reduction techniques like principal component analysis and singular value decomposition, RBF is non-reliant on training data or covariance structures, enabling greater flexibility and generalizability across diverse fracture morphologies and monitoring conditions.

Overall, this work offers an efficient and robust inversion algorithm, and opens up new methodological pathways for hydraulic fracture monitoring and intelligent diagnostics. For the domain of high-resolution, real-time fracture interpretation, the RBF-based dimension reduction approach significantly enhances inversion accuracy while reducing computational burden, making high-fidelity, low-latency geometry reconstruction feasible for field deployment. These findings lay a theoretical and algorithmic foundation for real-time monitoring and optimization in hydraulic fracturing, with strong implications for broader industry application and technological advancement.

Acknowledgements

The authors at China University of Petroleum, Beijing would like to acknowledge the support provided by the National Natural Science Foundation of China (Nos. 52320105002, 52421002 and 52374017), Science Foundation of China University of Petroleum, Beijing (No. 2462025YJRC017).

Supplementary file

https://doi.org/10.46690/ager.2025.06.06

Conflict of interest

The authors declare no competing interest.

References

Abdelaziz, A., Ha, J., Li, M., et al. Understanding hydraulic fracture mechanisms: From the laboratory to numerical modelling. Advances in Geo-Energy Research, 2023, 7(1): 66-68.

Al-Jahdhami, M. H., Chávez, C. A., Desouky, M. Fiber-optic deployed behind cemented casing in a vertical well for hydraulic fracture evaluation. SPE Journal, 2021, 26(2): 1058-1072.

Bertulessi, M., Bignami, D. F., Boschini, I., et al. Monitoring strategic hydraulic infrastructures by Brillouin distributed fiber optic sensors. Water, 2022, 14(2): 188.

Buhmann, M. D. Radial basis functions. Acta Numerica, 2000, 9: 1-38.

Byerley, G., Monk, D., Aaron, P., et al. Time-lapse seismic monitoring of individual hydraulic frac stages using a downhole DAS array. The Leading Edge, 2018, 37(11): 802-810.

Chen, R., Zaghloul, M. A. S., Yan, A., et al. High resolution monitoring of strain fields in concrete during hydraulic fracturing processes. Optics Express, 2016, 24(4): 3894-3902.

Ciezobka, J. Overview of hydraulic fracturing test site 2 in the Permian Delaware Basin (HFTS-2). Paper URTeC-5070 Presented at Unconventional Resources Technology Conference, Houston, Texas, USA, 26-28 July, 2021.

Denney D. Distributed acoustic sensing for hydraulic-fracturing monitoring and diagnostics. Journal of Petroleum Technology, 2012, 64(3): 68-74.

Eyinla, D. S., Henderson, S. K., Emadi, H., et al. Optimization of hydraulic fracture monitoring approach: A perspective on integrated fiber optics and sonic tools. Geoenergy Science and Engineering, 2023, 2: 212441.

Feng, Q., Xu, S., Xing, X., et al. Advances and challenges in shale oil development: A critical review. Advances in Geo-Energy Research, 2020, 4(4): 406-418.

Garavand, A., Podgornov, V. M. Hydraulic fracture optimization by using a modified pseudo-3D model in multi-layered reservoirs. Journal of Natural Gas Geoscience, 2018, 3(6): 401-410.

Gurjao, S. A., Gildin, E., Strecker, T. Estimation of far-field fiber-optics distributed acoustic sensing (DAS) response using physics-informed neural networks. SPE Journal, 2022, 27(4): 2735-2751.

Hudson, T. S., Baird, A. F., Kendall, J. M., et al. Distributed Acoustic Sensing (DAS) for natural microseismicity studies: A case study from Antarctica. Journal of Geophysical Research: Solid Earth, 2021, 126(7): e2020JB021493.

Hu, X., Tu, Z., Zhou, F., et al. A hydraulic fracture geometry inversion model based on distributed-acoustic-sensing data. SPE Journal, 2023, 28(3): 1560-1576.

Ismail, A., Azadbakht, S. A comprehensive review of numerical simulation methods for hydraulic fracturing. International Journal for Numerical and Analytical Methods in Geomechanics, 2024, 48(5): 1433-1459.

Leggett, S., Sakaida, S., Zhu, D., et al. Interpretation of fracture initiation points by in-well low-frequency distributed acoustic sensing in horizontal wells. SPE Journal, 2023, 28(5): 2583-2592.

Liao, Q., Wang, B., Chen, X., et al. Reservoir stimulation for unconventional oil and gas resources: Recent advances and future perspectives. Advances in Geo-Energy Research, 2024, 13(1): 7-9.

Liu, Y., Jin, G., Tinni, A., et al. Hydraulic-fracture-width inversion using low-frequency distributed-acoustic-sensing strain data-Part I: Algorithm and sensitivity analysis. Geophysics, 2020a, 85(6): KS149-KS161.

Liu, Y., Jin, G., Tinni, A., et al. Hydraulic-fracture-width inversion using low-frequency distributed-acoustic-sensing strain data-Part II: Extension for multifracture and field application. Geophysics, 2021a, 86(2): KS47-KS59.

Liu, Y., Jin, G., Tinni, A. Quantitative hydraulic-fracture geometry characterization with low-frequency distributed-acoustic-sensing strain data: Fracture-height sensitivity and field applications. Geophysics, 2021b, 86(5): KS87-KS98.

Liu, Y., Liang, S., Jin, G., et al. Stochastic inversion for equivalent hydraulic fracture geometry using low-frequency distributed acoustic sensing data. Geophysical Journal International, 2024, 238(2): 1391-1406.

Liu, Y., Wu, K., Jin, G., et al. Rock deformation and strain-rate characterization during hydraulic fracturing treatments: Insights for interpretation of low-frequency distributed acoustic-sensing signals. SPE Journal, 2020b, 25(5): 2251-2264.

Mahmoud, A., Gowida, A., Aljawad, M. S., et al. Advancement of hydraulic fracture diagnostics in unconventional formations. Geofluids, 2021, 2021: 4223858.

Mjehovich, J., Srinivasan, A., Wang, W., et al. Quantitative analysis of hydraulic fracturing test site 2 completion designs using crosswell strain measurement. SPE Journal, 2024, 29(5): 2303-2317.

Moradi, S., Angus, D. A., Verdon, J. P. Hydraulic fracture width inversion using simultaneous multiwell DAS strain data. Geophysical Journal International, 2022, 231(3): 1885-1900.

Paknia, F., Ghassemi, A., PourNik, M. A semi-analytical boundary element method to modeling and simulation of fluid-driven single/multi fractures in reservoirs. Paper SPE 196653 Presented at SPE Liquids-Rich Basins Conference-North America, Odessa, Texas, USA, 7-8 November, 2019.

Paullo, L., Mejía, C., Rueda, J., et al. Pseudo-coupled hydraulic fracturing analysis with displacement discontinuity and finite element methods. Engineering Fracture Mechanics, 2022, 272: 108774.

Sakaida, S., Pakhotina, I., Zhu, D., et al. Evaluating effects of completion design on fracturing stimulation efficiency based on DAS and DTS interpretation. Paper SPE 209143 Presented at SPE Hydraulic Fracturing Technology Conference and Exhibition, The Woodlands, Texas, USA, 1-3 February, 2022.

Sherman, D., Mellors, R., Ajo-Franklin, J. Geomechanical modeling of distributed fiber-optic sensor response to hydraulic fracturing. Journal of Geophysical Research:

Solid Earth, 2019, 124(3): 2480-2496.

Shou, K. J. A higher order three-dimensional displacement discontinuity method with application to bonded half-space problems. Minneapolis, University of Minnesota, 1993.

Srinivasan A., Liu Y., Wu K., et al. Geomechanical modeling of fracture-induced vertical strain measured by distributed fiber-optic strain sensing. SPE Production & Operations, 2023, 38(3): 537-551.

Staněk, F., Jin, G., Simmons, J. L. Fracture imaging using DAS-recorded microseismic events. Frontiers in Earth Science, 2022, 10: 907749.

Sun, Q., Tan, H., Zhang, Y., et al. A feasibility study on time-lapse controlled-source electromagnetic method for hydraulic fracturing monitoring of Well Eyangye-2HF in Yichang, Hubei Province, China. Journal of Geophysics and Engineering, 2023, 20(5): 1065-1075.

Tang, H., Wang, S., Zhang, R., et al. Analysis of stress interference among multiple hydraulic fractures using a fully three-dimensional displacement discontinuity method. Journal of Petroleum Science and Engineering, 2019a, 178: 595-611.

Tang, J., Wu, K., Zuo, L., et al. Investigation of rupture and slip mechanisms of hydraulic fractures in multiple-layered formations. SPE Journal, 2019b, 24(5): 2292-2307.

Tegtow, W., Boitz, N., Shapiro, S. A. Integrating microseismicity and low frequency DAS to characterize hydraulic fracturing. Geophysics, 2025, 90(3): M75-M84.

Wang, J., Tan, Y., Rijken, M., et al. Observations and modeling of fiber optic strain on hydraulic fracture height growth in Hydraulic Fracturing Test Site 2 (HFTS-2). SPE Journal, 2022a, 27(2): 1109-1122.

Wang, S., Chen, M., Lv, J. X., et al. Study of the evolution characteristics of fiber-optic strain induced by the propagation of bedding fractures in hydraulic fracturing. Petroleum Science, 2024, 21(6): 4219-4229.

Wang Y., Wu Z., Wang F. Research progress of applying distributed fiber optic measurement technology in hydraulic fracturing and production monitoring. Energies, 2022b, 15(20): 7519.

Weng, X. Incorporation of 2D fluid flow into a pseudo-3D hydraulic fracturing simulator. SPE Production Engineering, 1992, 7(3): 331-337.

Wu K., Liu Y., Jin G., et al. Fracture hits and hydraulic-fracture geometry characterization using low-frequency distributed acoustic sensing strain data. Journal of Petroleum Technology, 2021, 73(7): 39-42.

Wu, Y., Richter, P., Hull, R., et al. Hydraulic frac-hit corridor (FHC) monitoring and analysis with high-resolution distributed acoustic sensing (DAS) and far-field strain (FFS) measurements. First Break, 2020, 38(6): 65-70.

Xiang, J. A PKN hydraulic fracture model study and formation permeability determination. College Station, Texas A&M University, 2012.

Xi, X., Yang, S., McDermott, C. I., et al. Modelling rock fracture induced by hydraulic pulses. Rock Mechanics and Rock Engineering, 2021, 54(8): 3977-3994.

Yang, M., Valk, P. P., Economides, M. J. Hydraulic fracture production optimization with a pseudo-3D model in multi-layered lithology. Paper SPE 153847 Presented at SPE/EAGE European Unconventional Resources Conference & Exhibition-From Potential to Production, Vienna, Austria, 20-22 March, 2012.

Zhang, X., Wu, B., Jeffrey, R., et al. A pseudo-3D model for hydraulic fracture growth in a layered rock. International Journal of Solids and Structures, 2017, 115: 208-223.

Zhang, Z., Fang, Z., Stefani, J., et al. Modeling of fiber-optic strain responses to hydraulic fracturing. Geophysics, 2020, 85(6): A45-A50.

Zhang, Z., White, M. C. A., Bai, T., et al. Characterizing microearthquakes induced by hydraulic fracturing with hybrid borehole das and three-component geophone data. IEEE Transactions on Geoscience and Remote Sensing, 2023, 61: 4501315.

Zhuang, X., Li, X., Zhou, S. Transverse penny-shaped hydraulic fracture propagation in naturally-layered rocks under stress boundaries: A 3D phase field modeling. Computers and Geotechnics, 2023, 156: 105205.